

Solar sail formation flying for deep space remote sensing

James D. Biggs * Colin R. McInnes †

In this paper we consider how ‘near’ term solar sails can be used in formation above the ecliptic plane to provide platforms for accurate and continuous remote sensing of the polar regions of the Earth. The dynamics of the solar sail elliptical restricted three-body problem (ERTBP) are exploited for formation flying by identifying a family of periodic orbits above the ecliptic plane. Moreover, we find a family of 1 year periodic orbits where each orbit corresponds to a unique solar sail orientation using a numerical continuation method. It is found through a number of example numerical simulations that this family of orbits can be used for solar sail formation flying. Furthermore, it is illustrated numerically that Solar Sails can provide stable formation keeping platforms that are robust to injection errors. In addition practical trajectories that pass close to the Earth and wind onto these periodic orbits above the ecliptic are identified.

Nomenclature

a	semi-major axis
\mathbf{a}_s	solar sail acceleration (m/s^2)
a_x, a_y, a_z	components of solar sail acceleration (m/s^2) such that $\mathbf{a}_s = (a_x, a_y, a_z)^T$
e	eccentricity of the Earth’s orbit about the Sun $e = 0.0167$
f	true anomaly of the Earth about the Sun (radians)
G	universal gravitational constant ($6.673 \times 10^{-11} m^3 kg^{-1} s^{-2}$)
m_1	mass of the Sun (1.98892×10^{30} kg)
m_2	mass of the Earth (5.9742×10^{24} kg)
\hat{n}	unit normal to the sail
p	semi-latus rectum

*james.biggs@strath.ac.uk, Research Fellow, Department of Mechanical Engineering, James Weir Building, 75 Montrose Street, University of Strathclyde, Glasgow G1 1XJ.

†colin.mcinnnes@strath.ac.uk, Professor, Department of Mechanical Engineering, James Weir Building, 75 Montrose Street, University of Strathclyde, Glasgow G1 1XJ, member AIAA.

t^*	dimensionless time
\mathbf{r}	position vector of the solar sail in the rotating frame (AU)
\mathbf{r}_1	position of the Solar Sail with respect to the Sun (AU)
\mathbf{r}_2	position of the Solar Sail with respect to the Earth (AU)
\mathbf{V}	velocity vector of the Solar Sail
X, Y, Z	rotating coordinate frame (AU)
x, y, z	rotating-pulsating coordinate frame (AU)
β	solar sail lightness number - ratio of solar sail radiation pressure acceleration to solar gravitational acceleration $\beta = 0.05$
δ	the angle that the sail normal makes with the y -axis (radians)
γ	the angle that the sail normal makes with the x -axis (radians)
ρ	distance between the Sun and the Earth (AU)
μ	dimensionless mass of the Earth $\mu = 3 \times 10^{-6}$
$\boldsymbol{\omega}$	angular velocity vector of the rotating frame

1. Introduction

In this paper we propose solar sail propelled spacecraft flying in formation high above the libration point L_1 as platforms for remote sensing of the polar regions. Such deep space platforms allow for continuous remote sensing over large areas of the Earth - a viewpoint that is not possible from Low Earth Orbit (LEO) or Geosynchronous Earth Orbit (GEO) satellites. This provides a comprehensive and synoptic view of the Earth enabling the development of our understanding of the Earth's climate system. Such Earth observations from L_1 are both useful and feasible for remote sensing as highlighted in the Triana mission concept.¹ A solar sail which utilizes solar radiation for propulsion is known to be effective in maintaining orbits about and above such Libration points.²⁻⁴ Using the solar sail in these regions is advantageous as it can prolong mission duration extensively as the sail is not limited by propellant mass. In this paper we further exploit the solar sail's dynamics by considering its potential for formation-flying in deep space.

Solar sail propelled formation flying has the potential to enhance space-based imaging/interferometry missions by distributing mission tasks to multiple satellites. Incorporating this technology into future space missions at, and high above L_1 , can enlarge the sensing aperture and increase versatility of future observation platforms. Moreover, formation flying can be used to measure continuously both surface reflectance and atmospheric optical thickness. At least two satellites are necessary for taking such measurements because a partially cloudy atmosphere is a semitransparent layer of unknown optical thickness and the surface reflectance is also unknown.⁷ One such example is the 'Crystal shape estimation method' which is used to

measure the radiative effects of cirrus clouds in climate models, and requires measurements taken from the same clouds using two (or more) satellites in formation.⁸

Solar sail propelled formation flying around heliocentric displaced orbits has been considered recently in Gong *et.al.*,¹⁰ although the regions they consider have no practical application for remote sensing of the Earth. Simanjuntak *et.al.*¹¹ have also used a similar derivation of the solar sail relative dynamics to consider formation control about the classical L_2 point. Additionally solar sail propelled spacecraft flying in formation about L_1 has been proposed for the Geostorm warning concept.⁹ In this concept a group of four solar sails are placed in a diamond arrangement adjacent to L_1 to achieve a multi-point measurement of the solar environment. However, in this paper we propose using solar sail formation flying to provide a platform for advanced remote sensing of the polar regions. Additionally we propose a new control design for formation flying based on the underlying dynamics of the solar sail ERTBP. This method of solar sail propelled spacecraft flying in formation has the advantage over previous methods⁹⁻¹¹ in that it does not require linearization about the leader satellite, it can accommodate a large number of sails in both close and large formations and requires only small, practically feasible, variations in each sail's orientation to maintain.

The methodology in this paper extends from the identification of a family of periodic orbits high above L_1 , where each orbit in the family has the same period. This class of family of orbits (each orbit having the same period) is unique to the solar sail restricted three-body problem in that they do not exist in the classical three-body problem. It is shown that this family of orbits can be exploited for formation control by initializing a number of solar sails on various nearby orbits within this family. Furthermore, as the sail's orbits are of the same period, the relative distance between each sail is small and bounded, thus ensuring a strong degree of formation rigidity.

This paper extends the work of Biggs *et.al.*⁶ who identify a 1 year periodic orbit high above the ecliptic plane in the solar sail elliptical restricted three-body problem (ERTBP). Biggs *et.al.*⁶ used the method of Lindstedt-Poincaré to obtain high-order approximations of periodic orbits above the ecliptic in the solar sail circular restricted three-body problem (CRTBP).³ Following this, the high-order approximations were used as an initial 'guess' in a differential corrector to obtain closed orbits in the full nonlinear model. Finally, a numerical continuation with the eccentricity as the continuation parameter was used to identify a 1 year periodic orbit above the ecliptic plane in the solar sail ERTBP. In this paper we extend this work by using a continuation method¹² to find a family of 1 year periodic orbits with the solar sail orientation angle γ as the continuation parameter. This paper investigates how this unique family of orbits can be exploited for formation flying and this is illustrated through a number of example formation configurations. In addition some practical problems of formation control are addressed such as station keeping and robustness of the formations to injection errors.

2. Equations of motion for the solar sail elliptical restricted three-body problem (ERTBP)

We will consider a rotating frame of reference in which the primary masses are fixed and use a coordinate transformation to the pulsating-rotating frame. The pulsating-rotating frame is convenient as the true anomaly appears in the equations of motion as the independent variable and therefore we do not need to solve Kepler's equation. We begin by deriving the Lagrangian equations of the solar sail ERTBP. In this case the small primary is orbiting the large primary on an elliptic orbit. This orbit complies with the two body Keplerian motion; the distance between the primaries is given through the conic equation $\rho = \frac{p}{1+e \cos f}$ where $p = a(1 - e^2)$. The rate of change of the true anomaly satisfies $\dot{f} = h/\rho^2$ where $h^2 = G(m_1 + m_2)p$. We assume that an appropriate set of units is introduced so that $G = 1$, $a = 1$ and the system has unit total mass. The position vector of the solar sail in the rotating frame is $\mathbf{r} = (X, Y, Z)^T$. The coordinate system rotates at a rate \dot{f} about the $\hat{\mathbf{z}}$ axis and therefore $\boldsymbol{\omega} = \dot{f}\hat{\mathbf{z}}$. It follows that:

$$\mathbf{V} = \dot{\mathbf{r}} + \boldsymbol{\omega} \times \mathbf{r} = [(\dot{X} - \dot{f}Y), \dot{Y} + \dot{f}X, \dot{Z}]^T \quad (1)$$

We define the constant $\mu = m_2/(m_1 + m_2)$ where m_1 is located at $(-\rho\mu, 0, 0)^T$ and m_2 is located at $(\rho(1 - \mu), 0, 0)^T$. The position of the solar sail with respect to the primaries is then expressed as $\mathbf{r}_1 = [X + \mu\rho, Y, Z]^T$ and $\mathbf{r}_2 = [X + (\mu - 1)\rho, Y, Z]^T$. The Kinetic energy is $K = \frac{1}{2}\{(\dot{X} - \dot{f}Y)^2 + (\dot{Y} + \dot{f}X)^2 + \dot{Z}^2\}$ with the potential energy $U = -\frac{(1-\mu)}{\|\mathbf{r}_1\|} - \frac{\mu}{\|\mathbf{r}_2\|}$, it follows that the Lagrangian is then

$$L = \frac{1}{2}\{(\dot{X} - \dot{f}Y)^2 + (\dot{Y} + \dot{f}X)^2 + \dot{Z}^2\} + \frac{(1-\mu)}{\|\mathbf{r}_1\|} + \frac{\mu}{\|\mathbf{r}_2\|}$$

With this Lagrangian the Euler-Lagrange equations with the addition of the solar sail acceleration \mathbf{a}_s gives:

$$\frac{d}{dt} \left(\frac{\partial L}{\partial \dot{\mathbf{r}}_i} \right) - \frac{\partial L}{\partial \mathbf{r}_i} = \mathbf{a}_{s_i} \quad (2)$$

where $i = x, y, z$ are the vectors components and \mathbf{a}_s is defined by:

$$\mathbf{a}_s = \frac{\beta(1-\mu)}{\|\mathbf{r}_1\|^2} (\hat{\mathbf{r}}_1 \cdot \hat{\mathbf{n}})^2 \hat{\mathbf{n}} \quad (3)$$

We define $\hat{\mathbf{n}}$ in terms of two angles γ and δ with respect to the rotating frame:

$$\hat{\mathbf{n}} = (\cos \gamma \cos \delta, \cos \gamma \sin \delta, \sin \gamma)^T \quad (4)$$

While a β value of order 0.3 – 0.4 is considered within the realm of possibility, to put the analysis in this paper well within the near-term we will consider very modest β values of order 0.05. In order to simplify equation (2), a transformation to rotating-pulsating coordinates is required.¹⁴ This transformation consists of normalizing time by $\sqrt{(m_1 + m_2)/\rho^3}$ and normalizing position by the instantaneous distance:

$$X = \rho x, \quad Y = \rho y, \quad Z = \rho z \quad (5)$$

then transforming time derivatives into derivatives with respect to the true anomaly yields

$$\frac{d(\cdot)}{dt^*} = \frac{d(\cdot)}{df} \frac{df}{dt^*} = \frac{d(\cdot)}{df} \dot{f}, \quad \frac{d\rho}{df} = \frac{pe \sin f}{(1 + e \cos f)^2} \quad (6)$$

The relationship between the dimensionless, time dependent and the dimensionless true anomaly-dependent velocities and accelerations are:

$$\begin{aligned} \dot{X} &= \frac{d(\rho x)}{dt^*} = \dot{f}(\rho' x + \rho x') = \frac{h}{p} [e \sin f x + (1 + e \cos f) x'] \\ \ddot{X} &= \ddot{\rho} x + (2\dot{\rho} + \rho \dot{f}) x' + \dot{f}^2 \ddot{x} \\ &= \frac{h^2}{p^2} [(1 + e \cos f) x'' + e x \cos f] (1 + e \cos f)^3 \end{aligned} \quad (7)$$

the calculations of \dot{Y} , \dot{Z} , \ddot{Y} , \ddot{Z} follow in the same way and substituting these values into (2) yield the compact equations:

$$\begin{aligned} x'' - 2y' &= \frac{1}{1+e \cos f} \left(\frac{\partial \Omega}{\partial x} + a_x \right) \\ y'' + 2x' &= \frac{1}{1+e \cos f} \left(\frac{\partial \Omega}{\partial y} + a_y \right) \\ z'' + z &= \frac{1}{1+e \cos f} \left(\frac{\partial \Omega}{\partial z} + a_z \right) \end{aligned} \quad (8)$$

where

$$\Omega = \frac{1}{2}(x^2 + y^2 + z^2) + \frac{(1 - \mu)}{\|\mathbf{r}_1\|} + \frac{\mu}{\|\mathbf{r}_2\|}$$

The equations of motion (8) contain the time explicitly i.e. through the true anomaly f and are therefore non-autonomous. This implies that any periodic solution of the solar sail ERTBP must have a period which is an integer multiple of 1 year. In the case of remote sensing applications periodic orbits of one year are most convenient for remote sensing of the Earth's poles. Moreover, an orbit with a yearly periodicity means that a sail over the polar region could change position on the ecliptic plane at the same rate as the seasonal changes on Earth. Therefore, an imaging instrument could look at any spot on the surface under the same zenith angle regardless of the season.³ Before proceeding with the identification of a family of 1 year orbits, we highlight that this analysis focuses on a near term solar sail with $\beta = 0.05$. However, one key parameter in remote sensing missions is the distance of the Earth from the platform. This parameter drives aperture, interferometry baseline, and resolution requirements, which in turn drive mission cost. As the value of the lightness number β will determine the distance of the Earth from the platform it will have a direct impact on mission costs. In Biggs *et.al.*⁶ and Waters and McInnes³ a plot of the artificial equilibria above the ecliptic for different values of β are given for the case of the solar sail circular ($e = 0$) restricted three body problem. These equilibrium points are then used as a starting point to generate periodic orbits in the solar sail restricted three-body problem. As each of these orbits center around the equilibrium points they provide a good approximation of the average distance of the periodic orbit from the Earth. To illustrate this, Table 1 gives the distance of the orbit from the the Earth in the x direction for various β given an average displacement of approximately 0.01 AU above the ecliptic (or an approximate average altitude of 1.49×10^6 km above the Earth) :

Table 1. The distance of the sail from the Earth along the x-axis for varying lightness number β

Lightness Number β	0.05	0.1	0.2	0.4	0.5
Distance from the Earth (AU)	0.0110	0.0085	0.0073	0.0064	0.006172
Distance from the Earth (km)	1,645,578	1,271,583	1,092,065	957,427	923,318

Therefore, for higher performing displaced sails it is possible to reduce the distance of the sail from the Earth.

3. A family of periodic orbits each with period 1 year

In this section a numerical continuation method is implemented with the solar sail orientation angle γ as the continuation parameter. The continuation algorithm is based on a monodromy variant of Newton's method.¹² The initial orbit which will serve as a starter in the numerical continuation is given in the solar sail ERTBP.⁶ In this section we find 1 year periodic orbits above the ecliptic in the solar sail ERTBP described by the nonlinear system $\dot{\mathbf{X}}(t) = \mathbf{F}(\mathbf{X}(t), t)$, where $\mathbf{X}(t) = (x, y, z, x', y', z')$. The initial conditions that yield a 1 year periodic orbit above the ecliptic in the solar sail ERTBP are:

$$\begin{aligned}
 x(0) &= 0.99026089328, y(0) = 0.00000002532, z(0) = 0.01497820749 \\
 x'(0) &= 0.00000000062, y'(0) = 0.00306117311 \\
 z'(0) &= -0.00000003900, f(0) = 0, \gamma = 0.809196, \delta = 0
 \end{aligned} \tag{9}$$

The Newton method starts with an orbit $\mathbf{X}(t)$ initialized at $t = 0$ on a surface of section. In our case we require that all orbits in the family be of the same period so the return map in the rotating-pulsating frame is defined by a T-map of period $f = 2\pi$. The monodromy variant of Newton's method provides a numerical algorithm for moving from the nearby trajectory to the periodic orbit itself. Moreover, the Newton method provides an iterative improvement to the choice of initial conditions for a periodic orbit:¹²

$$\mathbf{X}^*(0) = \mathbf{X}(0) + (I - M)^{-1}[\mathbf{X}(T) - \mathbf{X}(0)] \tag{10}$$

where $\mathbf{X}^*(0)$ is the improved initial condition and M is the monodromy matrix. One of the problems encountered with this Newton method is that the determinant of $(I - M)$ may be zero and therefore the inverse is not well defined. However, this problem is resolved by using the Moore-Penrose pseudo inverse.¹³ The implementation of Newton's method relies on the computation of the monodromy matrix as follows:

Let $\mathbf{\Gamma}(t)$ denote a periodic orbit with period $T = 2\pi$ which satisfies the condition $\mathbf{\Gamma}(T) = \mathbf{\Gamma}(0)$, by letting $\mathbf{x} = \mathbf{X}(t) - \mathbf{\Gamma}(t)$, we may linearize the nonlinear system about this periodic orbit, resulting in the variational equations

$$\dot{\mathbf{x}} = A(t)\mathbf{x}$$

where

$$A(t) = A(t + T) = \left. \frac{\partial \mathbf{F}}{\partial \mathbf{X}} \right|_{\mathbf{X}(t)=\Gamma(t)}$$

explicitly:

$$A(t) = \begin{pmatrix} 0 & I \\ J & \Omega \end{pmatrix}, \quad J = \begin{pmatrix} a & b & c \\ d & e & f \\ g & h & i \end{pmatrix}, \quad \Omega = \begin{pmatrix} 0 & -2 & 0 \\ 2 & 0 & 0 \\ 0 & 0 & 0 \end{pmatrix} \quad (11)$$

where

$$\begin{aligned} a &= \left. \frac{\partial \mathbf{F}_x}{\partial x} \right|_{\Gamma(t)}, & b &= \left. \frac{\partial \mathbf{F}_x}{\partial y} \right|_{\Gamma(t)}, & c &= \left. \frac{\partial \mathbf{F}_x}{\partial z} \right|_{\Gamma(t)} \\ d &= \left. \frac{\partial \mathbf{F}_y}{\partial x} \right|_{\Gamma(t)}, & e &= \left. \frac{\partial \mathbf{F}_y}{\partial y} \right|_{\Gamma(t)}, & f &= \left. \frac{\partial \mathbf{F}_y}{\partial z} \right|_{\Gamma(t)} \\ g &= \left. \frac{\partial \mathbf{F}_z}{\partial x} \right|_{\Gamma(t)}, & h &= \left. \frac{\partial \mathbf{F}_z}{\partial y} \right|_{\Gamma(t)}, & i &= \left. \frac{\partial \mathbf{F}_z}{\partial z} \right|_{\Gamma(t)} \end{aligned}$$

Recasting the variational equations in terms of the state transition matrix (or principle fundamental matrix) $\Phi = \partial \mathbf{X}(t)/\partial \mathbf{X}(0)$, we have

$$\dot{\Phi} = A(t)\Phi, \quad \Phi(0) = I$$

where Φ is a 6×6 matrix and $A(t) = A(t + T)$. The monodromy matrix M is then defined as $M = \Phi(T)$. The monodromy matrix M is computed at each iteration and Newton's method is successful in identifying a family of 1 year period orbits with γ as the continuation parameter. The continuation parameter is varied between approximately $0.386 < \gamma < 0.817$ to yield Figures 1 and 2. In each case the smaller value of γ corresponds the periodic orbit furthest from the Earth and the largest value of γ to the periodic orbit nearest the Earth, as illustrated in Table 2.

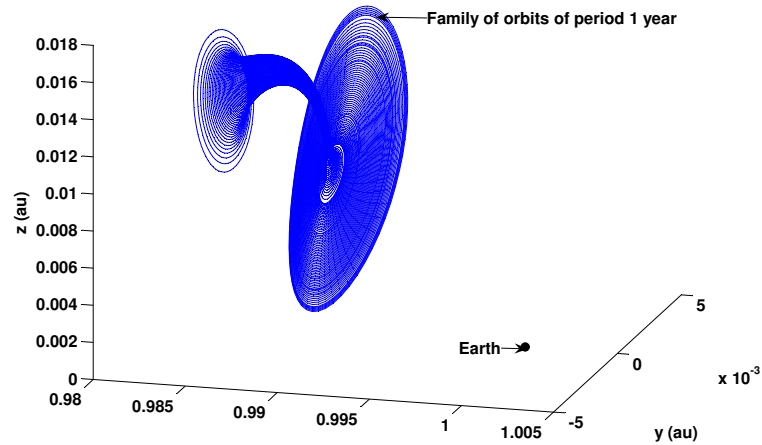


Figure 1. A family of orbits above the ecliptic plane.

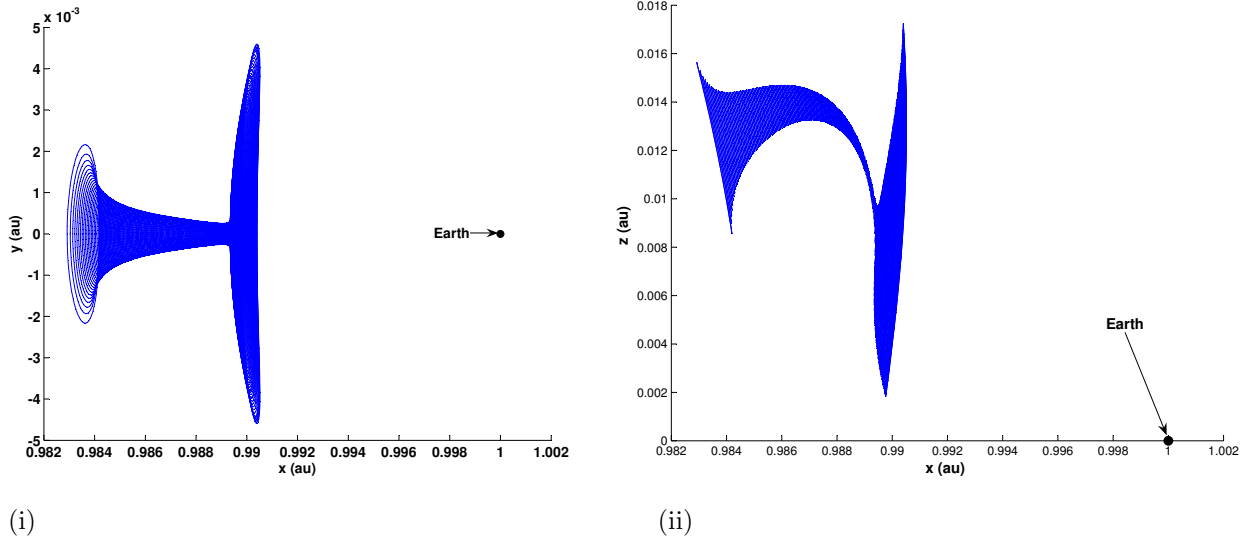


Figure 2. (i) The projection of Figure 1 onto the x-y plane. (ii) The projection of Figure 1 onto the x-z plane.

Table 2. The distance of the sail from the Earth along the x-axis for varying sail angle γ

Sail angle (γ)	0.368	0.438	0.614	0.76319	0.8164
Distance from the Earth (AU)	0.016497	0.015097	0.01281	0.010597	0.009697
Distance from the Earth (km)	2,467,918	2,258,481	1,916,350	1,585,290	1,450,651

In order to recreate some of these orbits we state the initial conditions required to produce the 1 year periodic orbit at approximately 2.5 million km from the Earth:

$$\begin{aligned}
 x(0) &= 0.98290573909134, y(0) = 0.00000000022241, z(0) = 0.01568674010849 \\
 x'(0) &= 0.00000000007113, y'(0) = 0.00218588428133 \\
 z'(0) &= -0.00000000037292, f(0) = 0, \gamma = 0.36795399999858, \delta = 0
 \end{aligned} \tag{12}$$

and the initial conditions required to produce the 1 year periodic orbit approximately 1.5 million km from the Earth:

$$\begin{aligned}
 x(0) &= 0.99040892177312, y(0) = 0.00000000677662, z(0) = 0.01765441016531 \\
 x'(0) &= 0.00000000058082, y'(0) = 0.00384425432531 \\
 z'(0) &= -0.00000001068849, f(0) = 0, \gamma = 0.81635569999972, \delta = 0
 \end{aligned} \tag{13}$$

The amplitude of these 1 year orbits in Figure 1 range from approximately 75,000 kilometers in radius to extremely large amplitudes of over 1 million kilometers in radius. The appropriate amplitude for the formation can therefore be chosen with a great deal of flexibility. In addition to this we will illustrate how this family of 1 year orbits can be used to design formations of sails which will further enhance remote sensing capabilities.

4. Solar Sail propelled spacecraft flying in formation

Formation flying has the advantage that it is possible to use small groups of less expensive, less complex satellites in place of singularly large, highly sophisticated platforms, such that a catastrophic failure does not necessarily cause irreparable harm to an overall mission. However, more significantly to this paper, solar sail formation flying has the potential to enhance space-based imaging/interferometry missions by distributing mission tasks to many small satellites. In this section the 1 year periodic orbits identified in Figure 1 are utilized for the purpose of formation flying. Initially it is shown that if two sails are placed close to one another on nearby orbits their relative motion will remain small and bounded. As the relative distance is bounded the formation will remain in an approximate rigid configuration.

4.A. Bounded relative solar sail motion

Using the family of 1 year periodic orbits we can place any number of sails in formation on a number of different orbits. As each of the orbits are of the same period the change in relative position will be bounded, as illustrated in Figures 3 and 4. In Figure 3 (i) two solar sail's are initialized on separate orbits at a distance of approximately 40 kilometers apart. It can be seen from Figure 3 (ii) the distance between the two solar sails remains small and bounded with a minimum separation of approximately 20 kilometers (lower bound) and a maximum separation of approximately 65 kilometers (upper bound). It is of course possible to place two sails on even closer orbits and in this case the absolute variation in separation is further reduced. For example two sails placed initially at 1 kilometer apart on different 1 year orbits in the family are shown to have a minimum of 0.6 kilometers and a maximum of 1.2 kilometers separation.

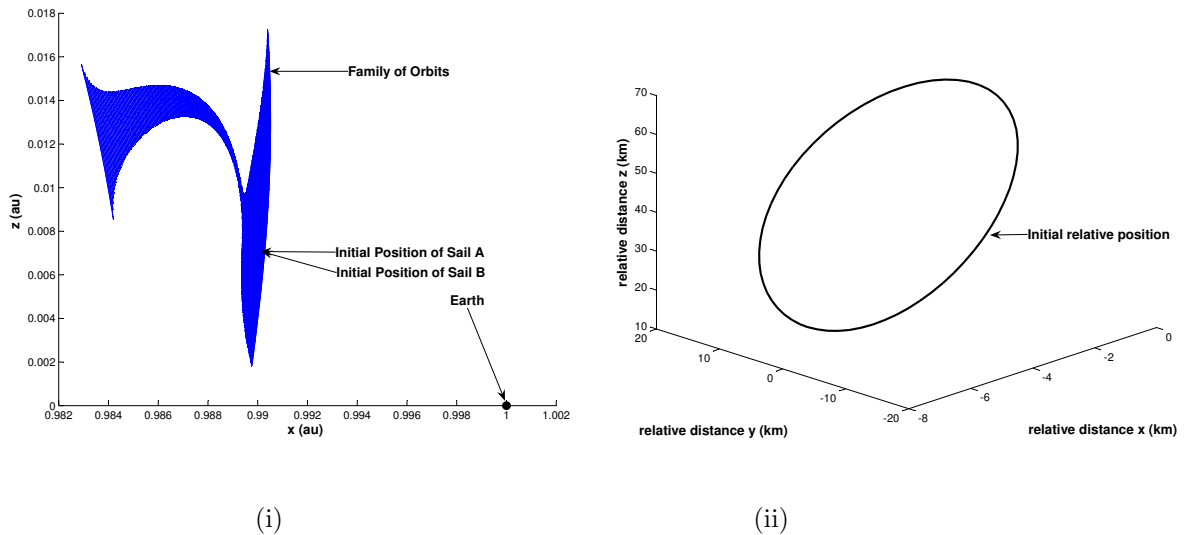


Figure 3. (i) Sail trajectories initialized 20 km apart. (ii) the relative distance between each sail.

In Figure 4 (i) two sails are initialized on separate orbits with large relative distance of approximately 400,000 kilometers. In this case the minimum separation is approximately 300,000 kilometers (lower bound) and a maximum separation of approximately 550,000 kilometers (upper bound). This illustrates that for large initial separation the variation in absolute terms is large but nevertheless bounded. The bounded relative distance of sails placed on orbits in this family imply that this region of phase space in the solar sail ERTBP would be useful for formation flying. In the following subsection we illustrate this with a number of simple examples.

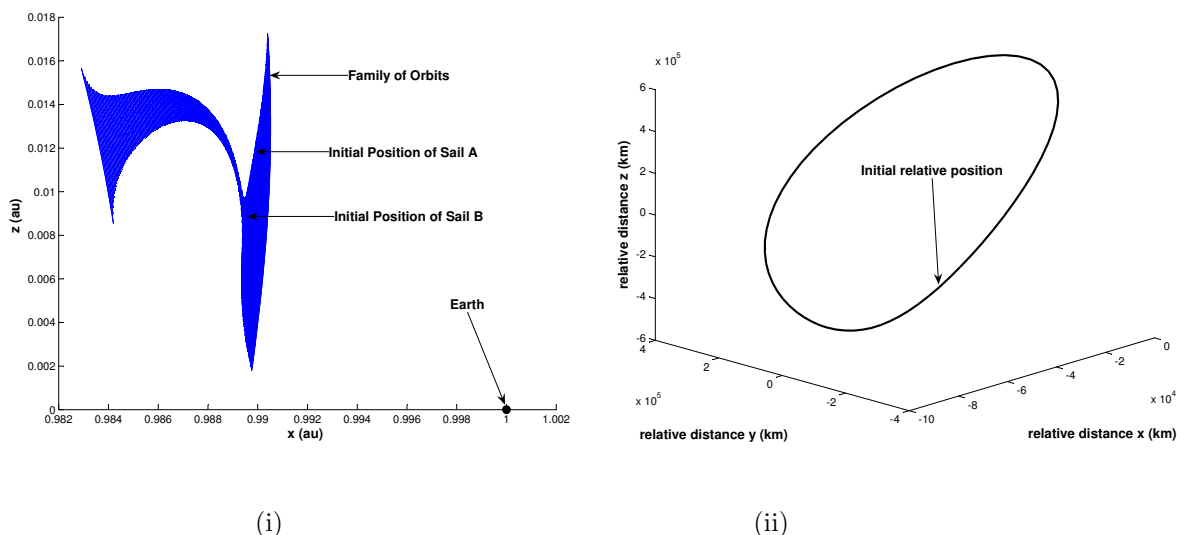


Figure 4. (i) Sail trajectories initialized 400,000 km apart. (ii) the relative distance between each sail.

4.B. Configurations for Formation flying

In this subsection we illustrate a number of simple formations that can be achieved and exploited for the purpose of remote sensing. Although small and large formations are equally achievable we illustrate formations that are spaced at large distances apart as their evolution in time can be clearly illustrated globally. There are two ways of positioning a solar sail on this family of orbits so that their relative distance remains small and bounded. Firstly, we can position two sails on the same periodic orbit, but at different initial positions on the orbit. This type of formation has the advantage that by flying the same trajectory and close together, nearly identical images taken by each satellite can be compared on the ground. Moreover, the leading satellite on the orbit will collect data and the follower satellite will refine the data through an atmospheric corrector.¹⁵ In other words a formation of satellites can gather, actual real time information about how the atmosphere distorts images from the ground and the sensors can then be calibrated to create significantly clearer images. This type of formation control can be implemented on any periodic orbit and an illustration is given in Figure 5 (i) with the orientation of the sails fixed at $\gamma = 0.8042$ rads and $\delta = 0$ rads.

A second way of positioning sails so that their relative distance remains small and bounded is by placing them on separate nearby orbits in the family. This is illustrated in Figure 5 (ii) which shows snapshots of two solar sails in formation as they motion around the 1 year orbits. This type of formation is possible for solar sails with different orientations i.e that induce different solar sail accelerations. In this example the sail on the inner orbit is oriented at $\gamma = 0.8042$ rads and $\delta = 0$ rads and the sail on the outer orbit is oriented at $\gamma = 0.809196$ rads and $\delta = 0$ rads.

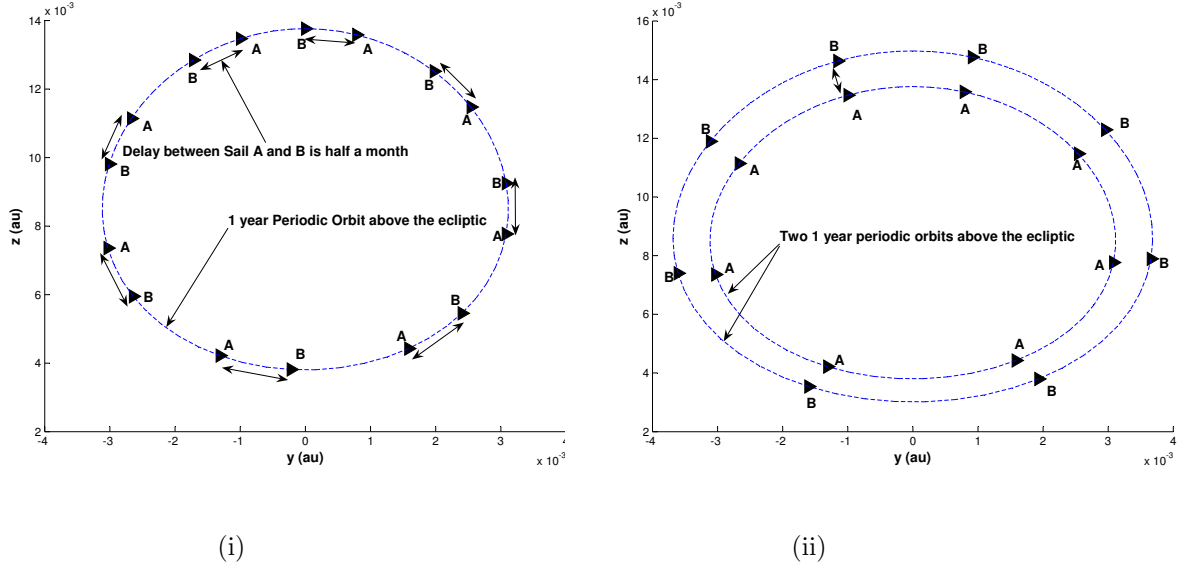


Figure 5. (i) Snapshots of two solar sails in a delayed formation. (ii) Snapshots of two solar sails in formation on separate orbits.

Finally, we can combine the two procedures of obtaining the formations in Figures 5 (i) and (ii) in order to achieve more complex formations. A simple triangular formation is illustrated in Figure 6. It is clear that more complex formations with a larger number of sails can also be formed using this family of 1 year orbits.

5. Practical control of solar sail formation flying

The 1 year periodic orbits illustrated in this paper are theoretically ideal regions in phase space to perform formation control. However, if such applications are to be implemented, we have to first consider some practical control issues. Firstly, the 1 year periodic orbits in Figure 1 are unstable; the characteristic exponents are of the form $\{\alpha_j, \bar{\alpha}_j, \alpha_i, \bar{\alpha}_i, \pm\alpha_r\}$ where $\bar{\alpha}$ denotes the complex conjugate of α and α_r is a real exponent. As the characteristic exponent α_r is much greater than 0 for these orbits they are highly unstable. In such a dynamically sensitive regime stabilization is required to counteract the effects of numerical error during the integration process, particularly when propagating the path over multiple revolutions. It is shown

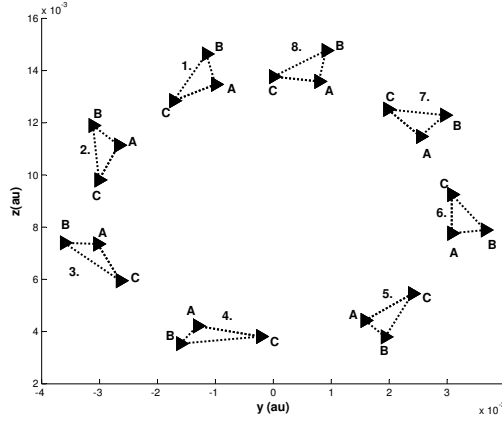


Figure 6. Snapshots of a triangular solar sail formation which can be maintained indefinitely.

in Biggs *et.al.*⁵ that the periodic orbit induced by the initial conditions (9) can be stabilized using small variations in the solar sail's orientation about $\gamma = 0.809196, \delta = 0$ and within the sail's maximum deflection rate of 1 degree per hour (a modest estimate). This procedure can be used to stabilize any of the 1 year periodic orbits in Figure 1. In this Section we proceed to investigate the robustness of the sail's ability to stabilize its motion on a 1 year orbit subject to initial orbit injection errors.

We proceed by using a continuous (time-varying) LQR controller in the solar sail ERTBP to track a periodic reference orbit using variations in the sail's orientation. The physical constraints to be considered are the sail's maximum deflection (radians) $-\pi/2 \leq \gamma, \delta \leq \pi/2$ (the sail has only one reflective side) and its maximum rate of deflection (radians per day) is $-0.42 \leq (\dot{\gamma}, \dot{\delta}) \leq 0.42$ (1 degree per hour). To begin we linearize the equations of motion about the reference orbit $\Gamma(t)$ and its corresponding solar sail orientation $\mathbf{u}_e = (\gamma_e, \delta_e)^T$. The reference orbit of each sail $\Gamma(t)$ corresponds to a particular orbit in the family. The most appropriate choice of nominal orbit within this family would be dependent on the remote sensing missions and required formation i.e desired distance from the Earth and relative distances between each spacecraft. Writing $\mathbf{x} = \mathbf{X}(t) - \Gamma(t)$ and $\Delta \mathbf{u} = \mathbf{u}(t) - \mathbf{u}_e$ then we can write the linear time-varying system as:

$$\dot{\mathbf{x}} = A(t)\mathbf{x} + B\Delta \mathbf{u} \quad (14)$$

where

$$A(t) = \partial f(\mathbf{X}(t), \mathbf{u}(t)) / \partial \mathbf{X} |_{\mathbf{X}(t)=\Gamma(t)}, \quad B = \partial f(\mathbf{X}(t), \mathbf{u}(t)) / \partial \mathbf{u}(t) |_{\mathbf{u}(t)=\mathbf{u}_e}$$

The linear state feedback control law which minimizes the quadratic cost function $J = \int_0^{\infty} \mathbf{x}^T Q \mathbf{x} + \partial \mathbf{u}^T R \partial \mathbf{u} dt$ where Q, R are symmetric positive semi-definite weighting matrices is given by $\Delta \mathbf{u} = -K\mathbf{x}$ with the time-varying gains matrix $K = R^{-1}B^T P(t)$ where $P(t)$ is the unique, positive semi-definite solution to the differential Riccati equation:

$$A(t)^T P(t) + P(t)A(t) - P(t)BR^{-1}B^T P(t) + Q = \dot{P}(t) \quad (15)$$

The weights Q and R are free to choose and for simplicity this freedom is reduced to one parameter by letting $Q = I_6$ and $R = kI_2$, where k is a constant. Therefore, the control effort will be penalized if k is large and the distance from the orbit will be penalized if k is small. The procedure used in this paper to determine Q and R is to solve equation (15) for $\dot{P}(t) = 0$ at $t = 0$ to obtain a constant K matrix. We then vary Q and R until we obtain a K that gives us the best control performance. Having obtained the most appropriate constant K we compute the corresponding P matrix through the equation $P = BRK$. This P will then serve as the initial condition $P(0)$ in the numerical integration of (15) to give the true optimal gains matrix for the linear time-varying system. We consider random initial injection errors and set the velocity error threshold to approximately ± 200 m/s. It was found that for these initial velocity errors a sail placed within 100,000 km of the orbit would converge to and stabilize its motion on the orbit. However, in many cases it was possible to achieve convergence with injection errors that induce much larger initial position errors (over 1,000,000 km can be achieved). This robustness to injection errors is due to the fact that the sails are operating within a vicinity of low pseudo gravity potential. This robustness is illustrated in the following example shown in Figure 7. We note that the active control remains within the sail's maximum deflection rate of 1 degree per hour

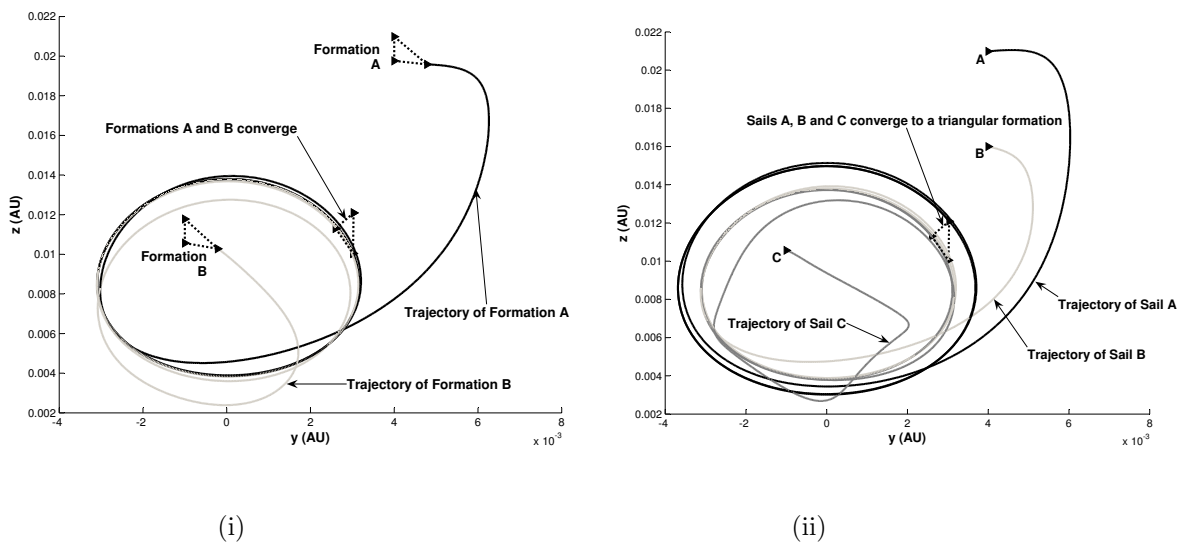


Figure 7. (i) Two triangular formations initialized with different and large injection errors.(ii) Three Sails initialized far apart in the vicinity of the 1 year periodic orbits.

In Figure 7 (i) two triangular formations are initialized with very different initial injection errors. In this case the two formations converge to the same formation on the 1 year orbits illustrating its robustness to initial injection errors. In addition it is illustrated in Figure 7 (ii) that three solar sails at large distances apart and with large injection errors converge to a triangular formation on the 1 year periodic orbits. This shows that even if the sail's are not initialized in formation and providing their reference trajectories are

adequately defined they will converge to their desired formation. In each of these cases the solar sail attitude angle does not violate its physical constraints of $-\pi/2 \leq \gamma, \delta \leq \pi/2$ and its maximum rate of deflection of 1 degree per hour. To give an indication of the magnitude and rate of the control we plot the attitude angles γ and δ required to drive the sail onto the reference and stabilize it over time (days) for the Sail A in Figure 7 (ii). This plot is illustrated in Figure 8 (i) over 500 days and it can be seen that for such a large perturbation the trajectory will converge to the reference orbit after approximately 1 year. It is clear from Figure 8 (i) that the largest deflection rates occur over the initial stage and converge to zero as the sail approaches the nominal orbit. To illustrate that the constraints are not being violated we plot the deflection rates over the first 5 days in Figure 8 (ii). In each case we fix the initial value of γ and δ equal to that required to settle on the reference orbit. As the sail is perturbed a large distance from the reference orbit the sail requires a large initial maximum rate of deflection which can be seen in Figure 8 (ii). The gradient of the curve in Figure 8 (ii) yields the deflection rate of the sail in radians per day and this can be seen to remain within the bound of $-0.42 \leq (\dot{\gamma}, \dot{\delta}) \leq 0.42$.

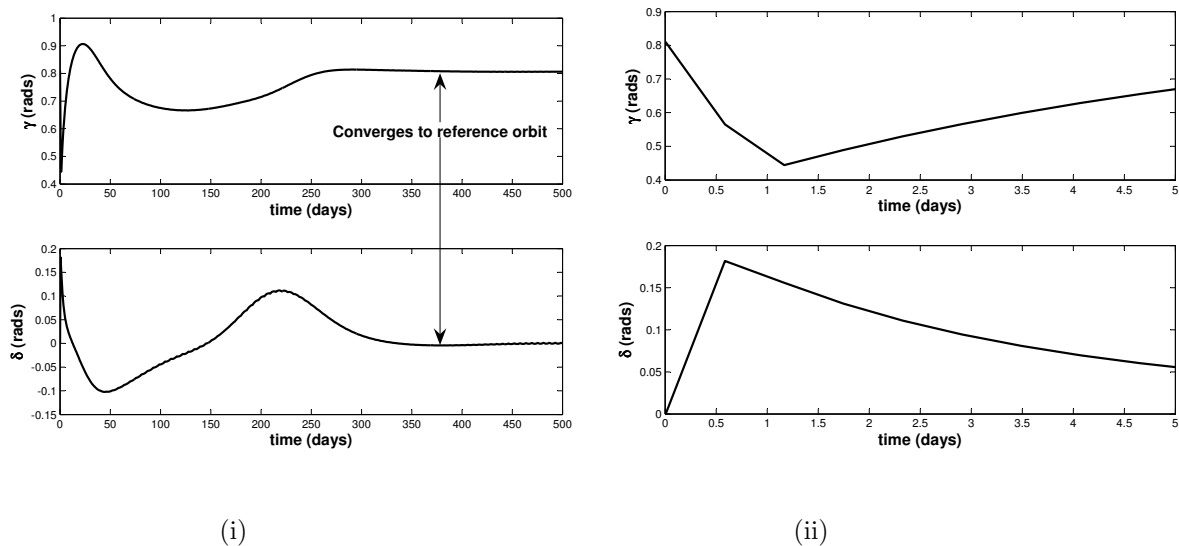


Figure 8. Control angles γ and δ (radians) over time (i) 500 days (ii) 5 days .

A final issue for the control of the sails is how to transfer them efficiently from the Earth to the 1 year periodic orbits above the ecliptic. This can be achieved by considering solar sail trajectories that pass close to the Earth along stable manifolds of the periodic orbits. The solar sail may be injected onto one of these trajectories and will then wind onto the periodic orbit using only solar radiation pressure for propulsion as illustrated in Figure 9. To obtain these trajectories we initialize the solar sail on the periodic orbit and backward integrate in the direction of the stable manifold. The time taken for a near Earth trajectory to arrive on a periodic orbit in Figure 9 is less than 8 months.

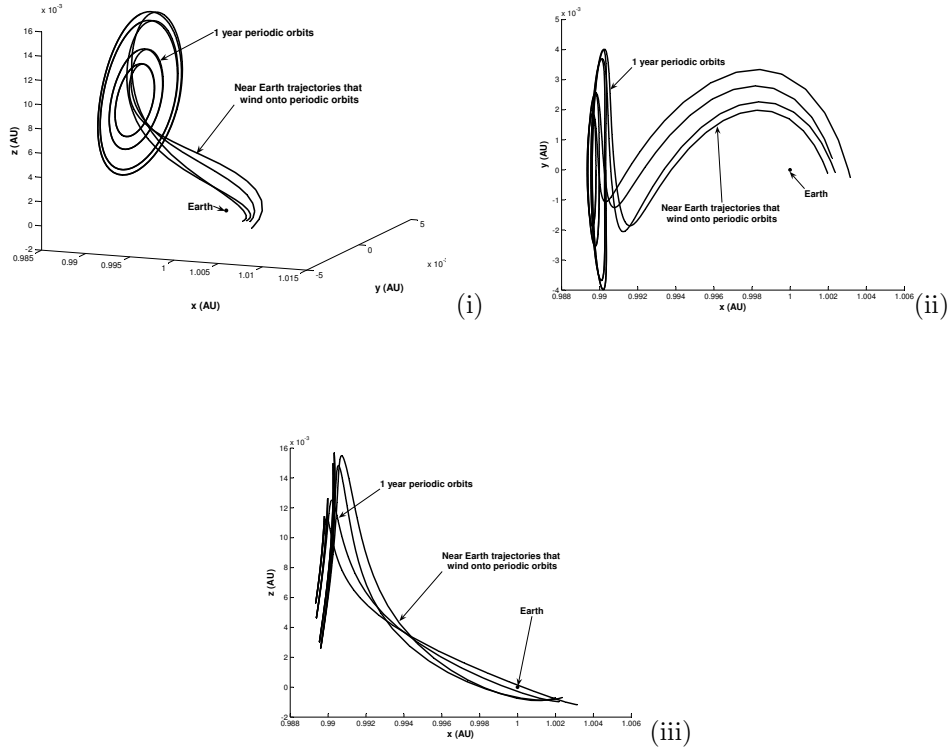


Figure 9. (i) Near Earth trajectories that wind onto orbits above the ecliptic plane. (ii) The projection of Figure 9 (i) onto the x-y plane. (iii) The projection of Figure 1 (i) onto the x-z plane.

In summary a number of ‘near term’ solar sails can be injected onto trajectories close to the Earth that will wind onto a family of orbits in a pre-specified formation.

6. Conclusion

In this paper it has been illustrated that ‘near’ term solar sails have the potential for robust formation flying above the ecliptic plane for the purpose of continuous remote sensing of the polar regions. A family of 1 year periodic orbits above the ecliptic in the solar sail elliptical restricted three-body problem is found using a numerical continuation method. It is shown through a number of numerical simulations that this family of orbits can be exploited for solar sail formation flying. It is illustrated that these formations are stable and robust to initial injection errors. Finally, the control of the sails into formation above the ecliptic is illustrated using trajectories that pass close to the Earth and that wind onto these periodic orbits.

Acknowledgments

This work was funded by grant EP/D003822/1 from the UK Engineering and Physical Sciences Research Council (EPSRC). The authors would like to thank Alex Coletti of SM Resources Corporation and Ben

Diedrich of NOAA Technology for their useful suggestions on the application of solar sail formation flying as platforms for remote sensing of the polar regions.

References

- ¹Watzin, J. 'The Triana Mission - next generation systems architecture ready for flight' Proceedings of the Aerospace Conference, vol. 7, pp. 277-285, 2000.
- ²McInnes, C. R., 'Solar sailing: technology, dynamics and mission applications'. Springer Praxis, 1999.
- ³Waters, T. J., McInnes, C. R., 'Periodic Orbits above the Ecliptic in the Solar Sail Restricted Three-body problem'. Journal of Guidance, Control and Dynamics, Vol. 30, No. 3, May-June, 2007.
- ⁴Bookless, J., McInnes, C. R., 'Control of Lagrange point orbits using Solar Sail propulsion'. Acta Astronautica, vol. 62, pp. 159-176, 2008.
- ⁵Biggs, J. D., McInnes, C. R., Waters, T., 'Control of Solar Sail Periodic orbits in the Elliptic three-body problem', Journal of Guidance, Control and Dynamics, vol. 32, No.1, pp. 318-320, 2009.
- ⁶Biggs, J. D., Waters, T. J., McInnes, C. R., 'New Periodic Orbits in the Solar Sail Three-body problem'. in Nonlinear Science and Complexity, Springer, 2009. [in press]
- ⁷King, M., *et. al.*, 'Remote Sensing of Tropospheric Aerosols from Space: Past, Present and Future' Bulletin of the American Meteorological Society, vol. 80, No. 11, pp. 2229-2259, 1999.
- ⁸Chepfer, H., *et. al.* 'Estimation of cirrus cloud effective ice crystal shapes using visible reflectances from dual-satellite measurements' Journal of Geophysical Research, vol. 107, No. D23, 4730, pp. 1-16, 2002.
- ⁹Sauer, C. G., 'The L_1 Diamond Affair' Proceedings of the 14th AAS/AIAA Space Flight Mechanics Conference, Hawaii, 2004.
- ¹⁰Gong, S., Baoyin, H., Junfeng, L., 'Solar Sail Formation Flying around displaced orbits' Journal of Guidance, Control and Dynamics, vol. 30, No.4, July-August 2007.
- ¹¹Siman, T., *et. al.*, 'Control strategies of formation flying using solar sail propulsion in the vicinity of collinear points' Proceedings of the 59th International Astronautical Conference, Glasgow, 2008.
- ¹²Marcinek, R., Pollak, E., 'Numerical methods for locating stable periodic orbits embedded in a largely chaotic system'. Journal of Chemical Physics, 100, 8, pp. 5894-5904, 1994.
- ¹³Campbell, S. L. and Meyer, C. D. 'Generalized Inverses of Linear Transformations'. New York: Dover, 1991.
- ¹⁴Szebehely, V., 'Theory of Orbits: The restricted problem of three bodies'. Academic Press, New York, 1967.
- ¹⁵Bauer, F., *et al.*, 'Satellite Formation Flying using an autonomous control system (AUTOCON) environment' Proceedings of the AIAA/AAS Astrodynamics Specialists conference, New Orleans, LA, 1997.